The Dissertation Committee for Andrew William Ritchie Certifies that this is the approved version of the following dissertation:

<Title of Dissertation or Treatise, Double-spaced, and centered, may be in ALL CAPITALS or Upper and Lower Case>

Committee:

Lauren J. Webb, Supervisor

Ron Elber

Walter Fast

Graeme Henkelman

Pengyu Ren

<Title of dissertation or treatise, double-spaced, may be in ALL CAPITALS or Upper and Lower Case, and centered>

by

Andrew William Ritchie, B.S. Chem

Dissertation

Presented to the Faculty of the Graduate School of

The University of Texas at Austin

in Partial Fulfillment

of the Requirements

for the Degree of

Doctorate of Philosophy

The University of Texas at Austin

August 2015

<Title of dissertation or treatise, double-spaced, and centered>

Andrew William Ritchie, PhD.

The University of Texas at Austin, 2015

Supervisor: Lauren J. Webb

<Abstract: May not exceed 350 words. It should be a continuous description, not disconnected notes or an outline.>

Table of Contents

List of Tables

List of Figures

List of Code and Parameters

Chapter 1 Introduction

<Body text to begin here.>

Chapter 2 Simulation Methods

2.1 Labeling and Mutating Proteins *in silico*

Simulation parameters for cyanocysteine and GDPNP were obtained from previous studies[1,2]. Simulations were performed using the Amber03 force field in Gomacs.[3] Ral structures from the 2RGF[4] crystal structure, Ras crystal structure from 1LFD[5], and Rap structures started from 1GUA[6].

Ralβ starting structures have previously been reported.[2] In short, all cysteine sidechain atoms except for Cβ were deleted from 2RGF and the sidechain was renamed to alanine. The C-terminal residues RTFT were taken from the pdb structure 1RAX (deposited in the PDB but unpublished) which ends in KKRTFT, and pasted onto the 2RGF structure, which ends in KKRT, by aligning the backbone atoms of the common KKRT residues and adding the FT coordinates onto the Ral structure file. The first residues in the 2RGF structure are ALA and LEU; these were changed to SER and HIS by renaming the residues in the pdb file, deleting hydrogen atoms, and renaming, using CD1 of LEU as ND1 of HIS. The N-terminal glycine (GLY 4) was modeled using Avogadro, completing the sequence. All missing heavy atoms were added using the tleap utility of Amber Tools.[7] The end resultant sequence is, starting from the N-terminal, GSH+Ral(2RGF,Cys→Ala)+FT.

To make Ras, the GAMGS sequence from chain B of 4K81[8] was used due to previous work which showed it to be the lowest energy conformation of this sequence available in the Protein Data Bank when bound to Ras.[9] The N-terminal methionine of 1LFD was aligned to the methionine immediately following the GAMGS sequence in 4K81, afterwhich the GAMGS coordinates were added to the Ras structure file. The end resultant sequence is GAMGS+Ras(1LFD).

Rap starting structures and mutations have also already been reported.[10] To start, a GSH tag left on the N-terminal methionine after cleavage of the hexa-histidine affinity label during protein purification was modeled onto the N-terminus. This was done by searching the Protein Data Bank for proteins starting with the sequence GSHM (Met is the first Rap residue present in 1GUA). 87 NMR structures and 1 crystal structure were obtained from pdbs 1AQ5 (20 NMR structures)[11], 1W9R (19 NMR structures)[12], 2WCY (48 NMR structures)[13], and 2VKJ (1 crystal structure)[14]. Rap was aligned to the methionine backbone of each GSHM structure using VMD[15], creating 88 structures containing the GSHM N-terminus. After adding hydrogen atoms using the GROMACS utility pdb2gmx[16], an energy minimization was performed and the lowest energy structure from this collection was chosen as the Rap model to be used for further calculations. The end resultant sequence is GSHM+Rap(1GUA). It was observed that in some structures, the N-terminal resides of Ralβ protruded between bonded atoms of Rap. To eliminate this nonphysical steric overlap, heavy atom restraints were placed on all but the Ralβ N-terminal GSHM residues and a 500 step gentle minimization was performed in Gromacs[16].

All side chain mutations were generated in the same manner using Amber Tools.[7] All side chain atoms except for shared heavy atoms were deleted from the mutation residue. The wild type residue was renamed to the desired residue and the resulting structure was passed to the tleap utility in Amber Tools[7] to model back in the missing atoms. In this way, starting from 1LFD Ras D30/E31K and 1GUA Rap E30D/K31E the additional Ras constructs D30/E31, D30E/E31, and D30E/E31K, and the additional Rap constructs E30/K31, E30D/K31, and E30/K31E were each constructed.

To generate cyanylated Ral structures $N27C_{SCN}$, $G28C_{SCN}$, $N29C_{SCN}$, $Y31C_{SCN}$, $K32C_{SCN}$, and $N54C_{SCN}$, residues were renamed to MET in the pdb file (because

methionine contains the same number of heavy atoms as cyanocysteine), retaining and renaming any atoms common to the native residue and methionine. Missing methionine atoms were added using tleap.[7] To complete the mutation to cyanocysteine, the MET atoms CG, SD, and CE were renamed SG, CD, and NE and a short energy minimization was performed.

To dock Rap to Ral, the alpha carbons of the GTPase units of 1LFD and 1GUA were first aligned using the Smith-Waterman algorithm[17] with a gap penalty of -3 (chosen because it gave results most consistent with the STAMP[18] structural alignment in VMD[15]), and the Ral coordinates were merged with the Rap coordinates of 1GUA and saved as a reference structure, Rap(1GUA)+Ral(1LFD). The mutated Rap structure was then aligned to the Rap unit of the Rap(1GUA)+Ral(1LFD) reference structure and the coordinates of the resulting Rap(mutant)+Ral(1LFD) were saved. To dock mutated Ras structures to Ral, the mutated Ras was aligned to the 1LFD Ras and the Ral coordinates were merged with the mutated Ras structure and the coordinates of the resulting Rap(mutant)+Ral(1LFD) were saved. To introduce the probe to the docked system, the cyanylated Ral was aligned to the Ral of each GTPase(mutant)+Ral(1LFD) reference structure, and the GTPase(mutant) coordinates were merged with the cyanylated Ral coordinates to create each GTPase+Probe construct: Ral+N27C_{SCN} , Ral+G28C_{SCN} , Ral+N29C_{SCN} , Ral+Y31C_{SCN} , Ral+K32C_{SCN} , Ral+N54C_{SCN} , Rap E30/K31+N27C_{SCN} , Rap E30/K31+G28C_{SCN} , Rap E30/K31+N29C_{SCN} , Rap E30/K31+Y31C_{SCN} , Rap E30/K31+K32C_{SCN} , Rap E30/K31+N54C_{SCN} , Rap E30/K31E+N27C_{SCN} , Rap E30/K31E+G28C_{SCN} , Rap E30/K31E+N29C_{SCN} , Rap E30/K31E+Y31C_{SCN} , Rap E30/K31E+K32C_{SCN} , Rap E30/K31E+N54C_{SCN} , Rap E30D/K31+N27C_{SCN} , Rap E30D/K31+G28C_{SCN} , Rap E30D/K31+N29C_{SCN} , Rap E30D/K31+Y31C_{SCN} , Rap E30D/K31+K32C_{SCN} , Rap E30D/K31+N54C_{SCN} , Rap E30D/K31E+N27C_{SCN} , Rap

E30D/K31E+G28C_{SCN} , Rap E30D/K31E+N29C_{SCN} , Rap E30D/K31E+Y31C_{SCN} , Rap E30D/K31E+K32C_{SCN} , Rap E30D/K31E+N54C_{SCN} , Ras D30/E31+N27C_{SCN} , Ras D30/E31+G28C_{SCN} , Ras D30/E31+N29C_{SCN} , Ras D30/E31+Y31C_{SCN} , Ras D30/E31+K32C_{SCN} , Ras D30/E31+N54C_{SCN} , Ras D30E/E31+N27C_{SCN} , Ras D30E/E31+G28C_{SCN} , Ras D30E/E31+N29C_{SCN} , Ras D30E/E31+Y31C_{SCN} , Ras D30E/E31+K32C_{SCN} , Ras D30E/E31+N54C_{SCN} , Ras D30/E31K+N27C_{SCN} , Ras D30/E31K+G28C_{SCN} , Ras D30/E31K+N29C_{SCN} , Ras D30/E31K+Y31C_{SCN} , Ras D30/E31K+K32C_{SCN} , Ras D30/E31K+N54C_{SCN} , Ras D30E/E31K+N27C_{SCN} , Ras D30E/E31K+G28C_{SCN} , Ras D30E/E31K+N29C_{SCN} , Ras D30E/E31K+Y31C_{SCN} , Ras D30E/E31K+K32C_{SCN} , and Ras D30E/E31K+N54C_{SCN} .

2.2 Enhanced Molecular Dynamics in Amber03: N-Dimensional Umbrella Sampling and Weighted Histogram Analysis Method

An umbrella sampling strategy was used to obtain a Boltzmann-weighted statistical ensemble of thiocyanate probe orientations for all MD sampling. Through examining simulated protein structures, it became increasingly apparent that a second degree of freedom, χ_1, was relevant to our probe conformational distributions. Therefore, two different umbrella sampling strategies were tested: one-dimensional sampling about the thiocyanate χ_2 dihedral angle and two-dimensional umbrella sampling about the thiocyanate χ_1 and χ_2 dihedral angles, shown in Figure 2-1. All molecular dynamics were completed using the GROMACS[16] software package at 300 K with the AMBER03[19] force field and periodic boundary conditions.

Six probe locations on RalGDS were examined: $N27C_{SCN}$, $G28C_{SCN}$, $N29C_{SCN}$, $Y31C_{SCN}$, $K32C_{SCN}$, and $N54C_{SCN}$, in the monomeric state and docked to each GTPase system examined. We have therefore examined all probe locations and mutated constructs for which experimental data are available. Six structures for each system modeled were generated by fixing the thiocyanate χ_2 dihedral angle from 0° to 300° in 60° increments. Each structure was sampled with a dihedral potential that was flat within ± 30° of the fixed-dihedral position and quadratic with a force constant of 1000 kJ mol^{-1} rad^{-2} otherwise. These restraining potentials were carried through for the duration of the system set-up and simulation. Each structure was energy minimized with cut-off electrostatics, solvated with tip3p water[11] in a dodecahedron box, charge balanced by randomly replacing the appropriate number of water molecules with sodium or chloride ions using the genion GROMACS utility, and solvent relaxed by sampling for 20 ps with position restraints on all non-solvent heavy atoms with a force constant of 1000 kJ mol^{-1} nm^{-2} using PME[20, 21] electrostatics with a real-space cut-off of 0.9 nm, spacing of 0.12 nm,

and interpolation order 4. Each rotamer of each system was then sampled using the GROMACS stochastic dynamics integrator, constraints on hydrogen-bonds using the LINCS algorithm[22], and PME electrostatics for 3 ns, recording snapshots every 5 ps, for a total of 18 ns of simulation and 3606 frames for each system.

Each frame was assigned to one of 72 5˚ bins from -180˚ to 175˚ based on the χ_2 dihedral angle. The weighted histogram analysis method (WHAM)[23, 24] was then used to calculate a torsional potential of mean force (PMF) for each of N bins i, which is related to the torsional probability distribution for each bin i (P_i) described by equation (2-1):

$$\mathrm{P}_i = \frac{e^{-\beta \cdot PMF_i}}{\sum_{j=0}^{N} e^{-\beta \cdot PMF_j}}, \ \beta = \frac{1}{k_b T} \tag{2-1}$$

which is the typical Boltzmann distribution function for a state i divided by the partition function, where T is the temperature in Kelvin, k_b is the Boltzmann constant, and PMF_j is the PMF for some state j.

The two-dimensional umbrella sampling was done in much the same way as the one-dimensional sampling, with few minor changes. The χ_1 angle was fixed from 0˚ to 300˚ in 30˚ increments, resulting in 12 structures. Each of these structures then had the χ_2 angle fixed from 0˚ to 300˚ in 30˚, resulting in 144 total structures. To avoid steric clashes in the starting structures, for each χ_2 rotation, the distance between the center of mass coordinate of each rotated atom and every non-rotated atom was calculated. If a distance was found to be under 1.5 Å, the χ_2 angle was rotated ± 1.5˚ from the dihedral center and the distances were recalculated. This was done until all non-bonded atoms were at least 1.5 Å from each rotated atom. Next, two harmonic dihedral restraining potentials were generated for each structure, one for the χ_1 dihedral angle and one for the χ_2 dihedral angle. Following the same set-up strategy used in the one-dimensional

sampling, the system was then energy minimized with cut-off electrostatics and dihedral force constants of 1000 kJ mol^{-1} rad^{-2}, solvated in tip3p water in a dodecahedron box, and charge balanced as described above. The system underwent solvent relaxation using PME electrostatics for 20 ps with a force constant of 1000 kJ mol^{-1} nm^{-2} on heavy backbone atoms, dihedral force constants of 150 kJ mol^{-1} rad^{-2}, and unrestrained side-chain atoms. Each of the 144 χ_1-χ_2 rotamers were then sampled for 400 ps using the GROMACS stochastic dynamics integrator with PME electrostatics (again, with a real-space cut-off of 0.9 nm, spacing of 0.12 nm, and interpolation order 4) and dihedral restraining potentials of 70 kJ mol^{-1} rad^{-2}, for a total of 57.6 ns of simulation and 11664 frames for each system. It is worth reiterating that each step used a progressively smaller dihedral restraining potential. This was done to ensure that the dihedral angles of the final structure before sampling were as close as possible to the umbrella-sampling window while still allowing nearby residues to relax to orientations that accommodate the inclusion of our probe. Starting with a large restraining potential fixes the probe to a specific location orientation and forcibly moves nearby residues to accommodate the probe to minimize interaction energies. Subsequent weakening of the restraining potential allows the probe to respond to its surroundings in a manner more typical of MD, allowing both the probe as well as the residues near the probe to relax to energy minimized orientations. Without this subsequent weakening, many simulations resulted in dihedral forces becoming larger than the integrator can or is expected to handle, which were usually caused by steric clashes between the probe and side-chain atoms.

A Boltzmann-weighted statistical ensemble of structures obtained from two-dimensional sampling was then assembled using WHAM. Each frame was assigned to one of 5184 5° by 5° bins. The bins were assigned based on equation (2-2), where b_1 is the one-dimensional χ_1 bin number, b_2 is the one-dimensional χ_2 bin number, B_i is the

total number of bins in degree of freedom *i* (72 for all two-dimensional sampling done), and i_{index} refers to the subscript on *b*. Conditional probability was assumed.

$$\mathrm{Bin}(b_1,b_2) = \sum_{i=b_1,\,b_2} B_i^{\,2-i_{\mathrm{index}}} \cdot i \tag{2-2}$$

To validate our 2D WHAM code, we examined a Ryckaert-Bellemans dihedral potential, shown in equation (2-3), where ϕ is some angle and n and C_n are some example parameters obtained from the GROMACS manual, shown in Table 2-1. This is a very simple potential function with no contributions from any other source, unlike the potential energy calculation in a protein, which will be influenced by various force field parameters such as bond force constants. However in WHAM, the sources of the potentials are not distinguished, and we are able to use the simple Ryckaert-Bellemans model to validate the code. We constructed the PMF from the sum of the potentials for a given pair of coordinates and the unbiased probability distribution, $p^{\circ}(\chi_1, \chi_2)$, using the ratio of the Boltzmann distribution function to the partition function, shown in equation (2-4), over an array of 2D dihedral angles ranging form -180° to 180°.

$$V_{rb} = \sum_{n=0}^{5} C_n \left(\cos\left(\phi - \pi\right)\right)^n \tag{2-3}$$

Next, we constructed the PMF and probability distribution landscapes, shown in Figure 2-1a. We then applied biasing potential windows to each dimension in a manner that mimics the methods used in GROMACS. The biased probability, $p(\chi_1, \chi_2)$, is given by equation (2-5). We then performed a Monte Carlo simulation centered on each of 144 biased windows, each with dimensions of 30° x 30°, with a probability $p(\chi_1, \chi_2)$ of sampling a given pair of dihedral angles, which was then analyzed using our 2D WHAM code to return the unbiased PMF and $p^{\circ}(\chi_1, \chi_2)$.

$$p^{\circ}(\chi_1,\chi_2) = \frac{e^{-\beta\left(V_{rb}(\chi_1)+V_{rb}(\chi_2)\right)}}{\int\int e^{-\beta\left(V_{rb}(\chi_1)+V_{rb}(\chi_2)\right)}\, d\chi_1\, d\chi_2} \tag{2-4}$$

$$p(\chi_1,\chi_2) = \frac{e^{-\beta\left(V_{rb}(\chi_1)+V_1+V_{rb}(\chi_2)+V_2\right)}}{\iint e^{-\beta\left(V_{rb}(\chi_1)+V_1+V_{rb}(\chi_2)+V_2\right)} d\chi_1 d\chi_2} \quad (2\text{-}5)$$

Figure 2-1 shows the analytical PMF and probability distributions (a), WHAM PMF and probability distributions on 144 windows each containing 40 frames (b), WHAM PMF and probability distributions on 144 windows each containing 80 frames (c), WHAM PMF and probability distributions on 144 windows each containing 160 frames (d), and WHAM PMF and probability distributions on 144 windows each containing 1000 frames (e). The major features of the probability distribution become clear after only 40 frames; after 80 frames the probability distributions look very similar to the analytical distribution, and after 160 frames very little improvement is seen. We can also see that the high probability regions, representing the staggered orientations, have PMF landscapes that look like the analytical PMF, although the gauche regions appear to be ill characterized still. After 1000 frames the probability distribution is nearly identical to the analytical distribution and the moderate ranges of the PMF (light blue, > 17.92 kJ mol^{-1}) now quantitatively approach the predictions of the analytical expression. Exact analytical PMF matching of low probability regions is very slow, requiring ≥10000 frames. From these results we conclude that the PMF converges to the analytical expression slowly for regions of low probability and quickly for regions of high probability.

Table 2-1: Sample Parameters for Ryckaert Bellemans dihedral potential function used for validating 2D WHAM code

	Constraint (kJ mol^{-1})		**Constraint (kJ mol^{-1})**
$\mathbf{C_0}$	9.28	$\mathbf{C_3}$	-3.06
$\mathbf{C_1}$	12.16	$\mathbf{C_4}$	-26.24
$\mathbf{C_2}$	-13.12	$\mathbf{C_5}$	-31.5

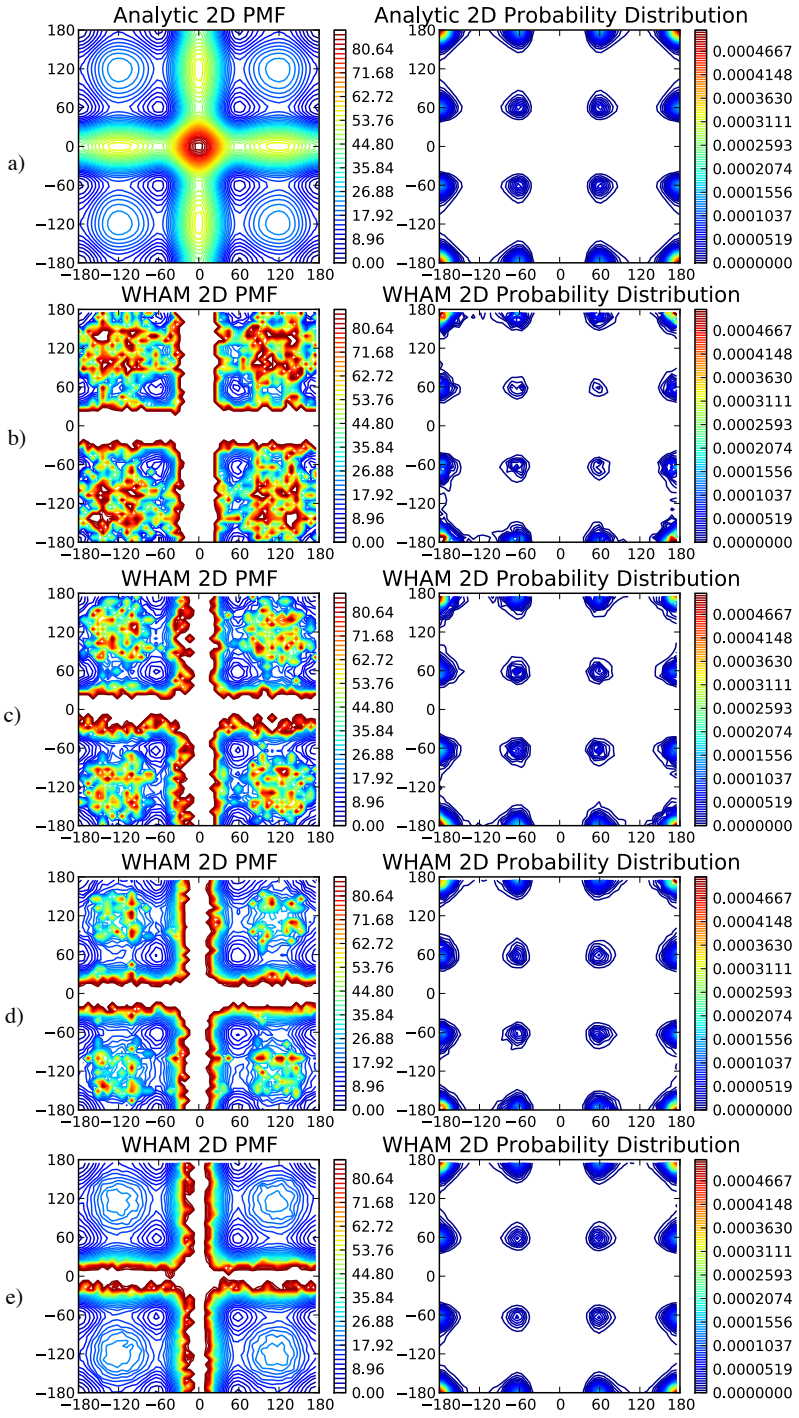

Figure 2-1: 2D WHAM Validation

Comparison between the PMF and probability distributions of a) an analytic Ryckaert-Bellemans dihedral potential and Monte Carlo 2D umbrella sampling for b) 40 frames/biasing window; c) 80 frames/biasing window; d) 160 frames/biasing window; e) 1000 frames/biasing window. Units on the PMF are kJ mol^{-1}.

2.3 Electrostatic Clustering in Vibrational Chromophore Dihedral Space

The largest bottleneck for these sorts of calculations we do are the electrostatics. A single node on Stampede can generate >10 ns of simulation per day. That number can be increased (logarithmically) by using additional nodes. However, the continuum solvent electrostatics calculations take anywhere from 45-60 seconds (APBS) to $\approx 20 minutes (AMOEBA) per frame. If we keep every 4 ps and collect 250 frames per nanosecond, then the electrostatics require 5-8 ns/day for APBS calculations and approximately 0.3 ns/day for AMOEBA calculations. This can be decreased further by running the serial calculations in parallel. Regardless, it would be convenient to find some method of pruning the total number of frames for continuum electrostatics calculations while ensuring that the average field does not differ significantly from the average using every frame.

For convenience, the vacuum electrostatic field at the nitrile due to solute only was chosen as an indicator of total electrostatic field. In the absence of solvent, this is trivial to calculate for both point charge force fields (Amber03) as well as multipole force fields (AMOEBA). This was chosen because it was 1) intuitive and 2) there is consistently a good correlation between the solute Coulomb field and the PB solvent reaction field, as seen in Figure 2-2,git suggesting that frames which well represent the Coulomb field also well represent the reaction field.

We then took advantage of the weighted averaging over binned data. The Boltzmann weighted average is calculated as in equation (2-6),

$$\langle x \rangle = \sum_{i=1}^{\text{nbins}} \rho_i \sum_{j=1}^{c_i} \frac{x_{ij}}{c_i} \tag{2-6}$$

where the probability of being in each bin i is ρ_i, the number of times bin i is visited is c_i, and each value in bin i is x_{ij} for $j = 1$ to $j = c_i$. There exists some subarray of

values in bin i that has k_i values, where $k_i \geq c_i$ entries and $\left| \sum_{j=1}^{k_i} \frac{x_{ij}}{k_i} - \sum_{j=1}^{c_i} \frac{x_{ij}}{c_i} \right| \leq \chi$, where χ is some threshold. As χ approaches 0, k_i approaches c_i, and the subarray is the full array and the averages are identical. Using the a set of test data where umbrella windows were centered every 120 degrees (at 60˚, 180˚, and 300˚, the expected alkane maximum probability torsions) with a flat biasing potential ± 60˚ of the window center and a force constant of **XXX, the clustered average field for each Ral probe in the monomeric state, docked to each of the four Rap1a mutants and each of the four Ras mutants is plotted against their average field for various values of χ, indicated in the upper-left corner of each subplot, from the full data sets in Figure 2-3. From this, it's clear that the clustered averages are linearly correlated to the full averages. The correlation coefficients and best-fit slopes have also been plotted as a function of the cutoff, χ, in Figure 2-4. Even for a relatively large $\chi = 1$, the clustered correlation coefficient and slope is *very* close to 1.0. In general, as χ approaches zero, the correlation coefficient and slope also approach zero. Moreover, at a $\chi = 0.01$, only approximately 20% of all frames are used, which is a significant decrease in computation requirement. This method also has the advantage of guaranteeing that the property the cluster is based on always has a clustered average nearly identical to the full average, which is a useful sanity check.

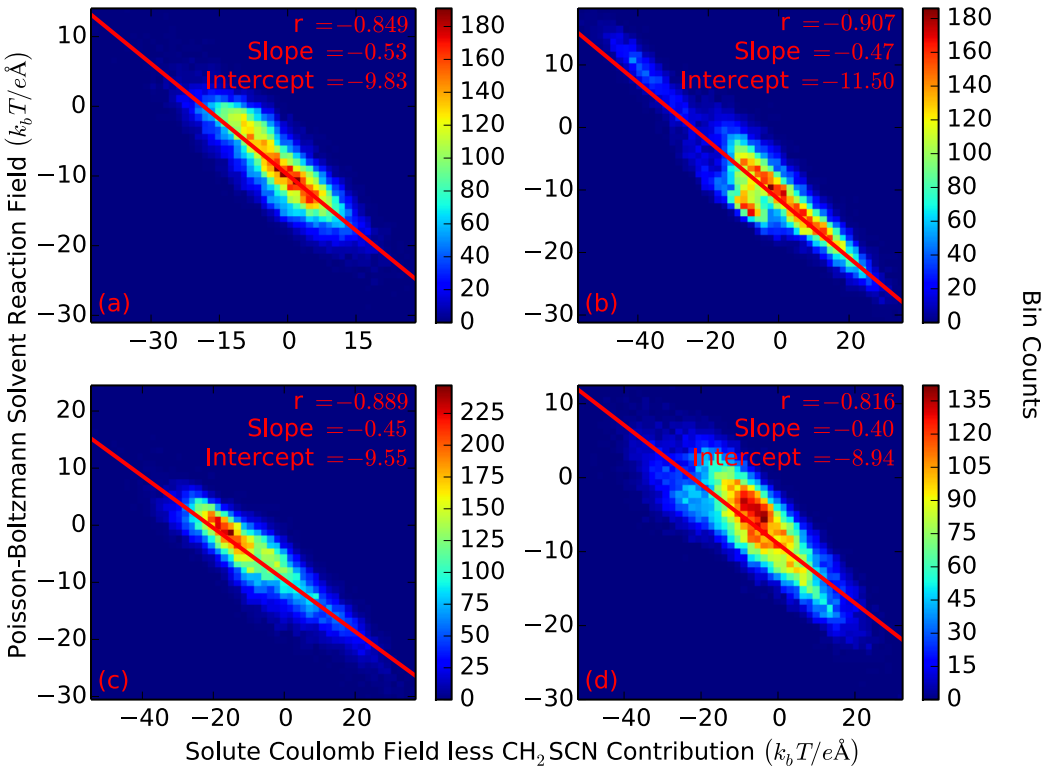

Figure 2-2: PB Solvent Reaction Field vs. Solute Analytic Coulomb Field

Comparison between the analytic Coulomb field at the nitrile bond midpoint due to solute (less the contributions due to the probe itself) (x-axis) and the solvent reaction field at the nitrile bond midpoint (y-axis) using Amber03 point charges for a) Ral $G28C_{SCN}$ monomer; b) Ral $N54C_{SCN}$ monomer; c) Ral $G28C_{SCN}$ docked to wild type Rap; d) Ral $N54C_{SCN}$ docked to wild type Rap. Correlation coefficients (r), slopes (m), and y-intercepts (int), are indicated in the upper-right corner of each figure.

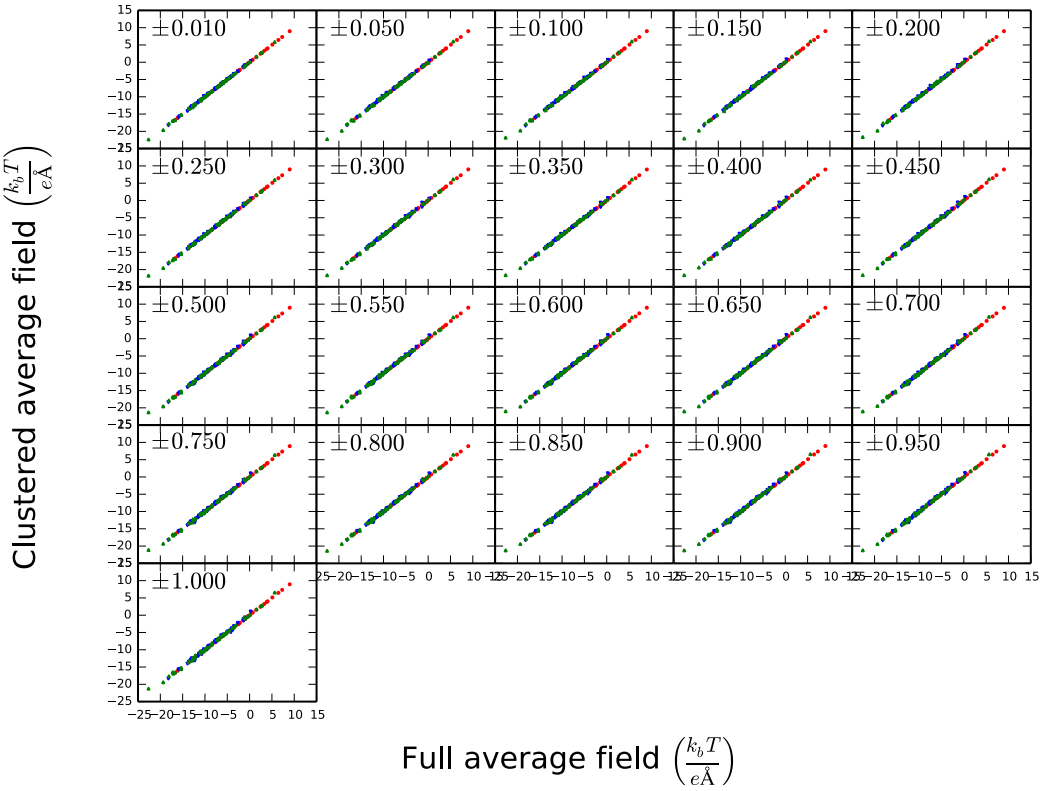

Figure 2-3: Field Values using Clustering Vs. Field Values using All Frames

Average Coulomb electrostatic field (red), solvent reaction field (blue), and the electrostatic field calculated using the AMOEBA force field (green) from clustered frames versus the respective full averages for various cutoff values, χ, indicated in the top left corner of each box.

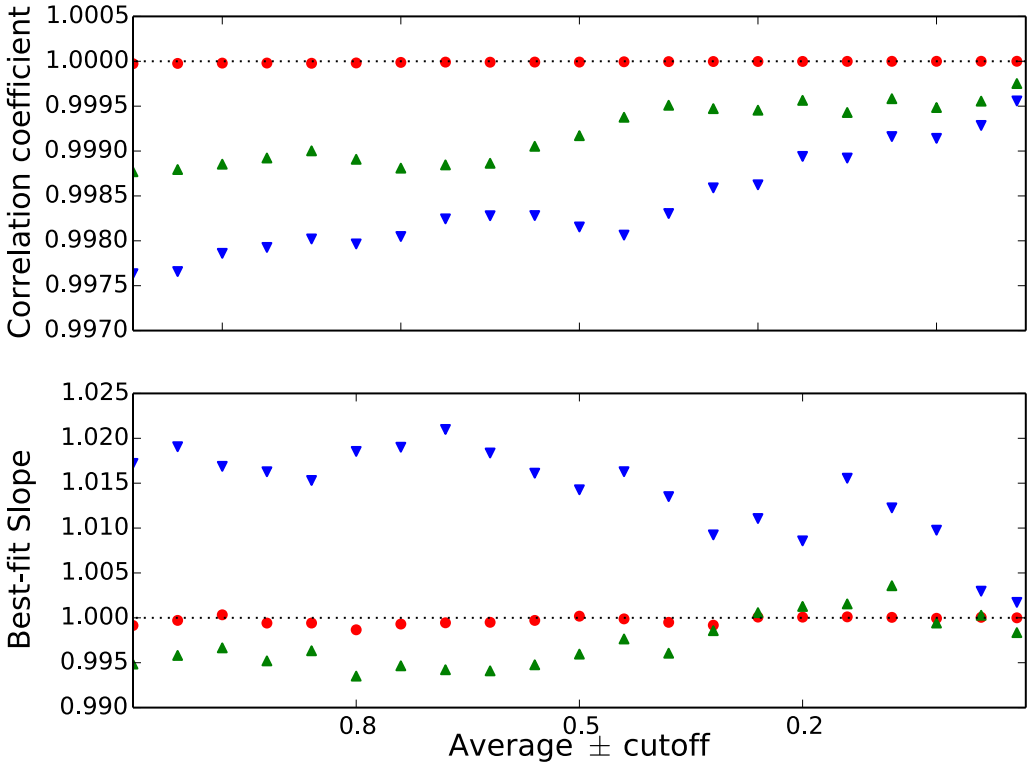

Figure 2-4: Correlations and Slopes at Various Cutoff Values

Correlation coefficients of the Coulomb electrostatic field (red), solvent reaction field (blue), and the electrostatic field calculated using the AMOEBA force field (green) as a function of the cutoff, χ. (Bottom) Best-fit slopes of the Coulomb electrostatic field (red), solvent reaction field (blue), and the electrostatic field calculated using the AMOEBA force field (green) as a function of the cutoff, χ.

2.4 PROBE PARAMETERIZATION FOR AMOEBA

<Body text to begin here.>

```
atom         259   55    CB    "CNC CB"                     6    12.011    4
atom         260   56    SG    "CNC SG"                    16    32.066    2
atom         261   57    CD    "CNC CD"                     6    12.011    2
atom         262   58    NE    "CNC NE"                     7    14.007    1
atom         263   59    HB    "CNC HB"                     1     1.008    1

multipole    259    8  260              -0.15228
                                         0.07407   0.00000   0.31740
                                        -0.15117
                                         0.00000  -0.21945
                                        -0.19282   0.00000   0.37062
multipole    260  259  261               0.33074
                                         0.44389   0.00000   0.28736
                                         1.22369
                                         0.00000  -2.16613
                                        -0.31636   0.00000   0.94244
multipole    261  260  262               0.24556
                                         0.06457   0.00000  -0.41800
                                         0.15740
                                         0.00000   0.22633
                                         0.26601   0.00000  -0.38373
multipole     12    8  259               0.12898
                                         0.02551   0.00000   0.07014
                                         0.19051
                                         0.00000   0.17012
                                        -0.01582   0.00000  -0.36063
multipole    263  259    8               0.09179
                                        -0.07114   0.00000  -0.02080
                                        -0.16061
                                         0.00000  -0.02258
                                        -0.03267   0.00000   0.18319
multipole    262  261  260              -0.58843
                                        -0.00512   0.00000  -0.24238
                                         0.32332
                                         0.00000   0.16836
                                        -0.08202   0.00000  -0.49168

polarize     259          1.3340     0.3900    263
polarize     260          3.3000     0.3900    261
polarize     261          1.3340     0.3900    260  262
polarize     262          1.0730     0.3900    261
polarize     263          0.4960     0.3900    259

vdw           58              3.7100     0.1050
vdw           55              3.7800     0.1060
vdw           56              4.0050     0.3550
vdw           57              3.7800     0.1060
vdw           59              2.8700     0.0330      0.900
bond          55    7        323.0000     1.5317
bond          55   56        235.8000     1.8353
bond          55   59        341.0000     1.0817
bond          56   57        235.8000     1.7060
bond          57   58        450.0000     1.1374
angle          7   55   56    53.2000   109.6948
angle          7   55   59    42.4400   110.8048
angle         56   55   59    60.2400   108.4887
angle         59   55   59    39.5700   108.8231
```

```
angle         55    7    3    60.0000   108.7411
angle         55    7    1    80.0000   112.9036
angle         55    7    6    38.0000   109.5706
angle         55   56   57    60.4300    98.5327
angle         56   57   58    60.0000   178.6763
strbnd         7   55   56    18.7000    18.7000
strbnd         7   55   59    11.5000    11.5000
strbnd        56   55   59    11.5000    11.5000
strbnd        55    7    3    18.7000    18.7000
strbnd        55    7    1    18.7000    18.7000
strbnd        55    7    6    11.5000    18.7000
strbnd        55   56   57    -5.7500    -5.7500
torsion       56   55    7    3     -
   1.010 0.0 1   1.230 180.0 2   1.000 0.0 3 # CYS 3 7 8 12
torsion       56   55    7    1     -0.160 0.0 1   1.080 180.0 2  -
   1.520 0.0 3 # CYS 1 7 8 12
torsion       56   55    7    6      0.000 0.0 1   0.000 180.0 2   0.475 0.0 3 #
   CYS 6 7 8 12
torsion       59   55    7    3      0.000 0.0 1   0.000 180.0 2   0.180 0.0 3 #
   CYS 3 7 8 9
torsion       59   55    7    1      0.000 0.0 1   0.000 180.0 2   0.500 0.0 3 #
   CYS 1 7 8 9
torsion       59   55    7    6      0.000 0.0 1   0.000 180.0 2   0.299 0.0 3 #
   CYS 6 7 8 9
torsion        7   55   56   57    -0.4400 0.0 1 -
   0.2600 180.0 2  0.6000 0.0 3 # EtSCN C1 C2 S C
torsion       59   55   56   57     0.0000 0.0 1  0.0000 180.0 2  0.6600 0.0 3 #
   EtSCN H2 C2 S C
torsion       55    7    3    1      0.929 0.0 1   0.328 180.0 2   0.000 0.0 3 #
   CYS 1 3 7 8
torsion       55    7    3    5      0.000 0.0 1   0.000 180.0 2   0.000 0.0 3 #
   CYS 5 3 7 8
torsion       55    7    1    3      2.576 0.0 1   1.011 180.0 2   0.825 0.0 3 #
   CYS 3 1 7 8
torsion       55    7    1    4      0.000 0.0 1   0.000 180.0 2   0.000 0.0 3 #
   CYS 4 1 7 8
torsion       55   56   57   58     0.0000 0.0 1  0.0000 180.0 2  0.5000 0.0 3 #
   EtSCN C2 S C N
```

Code and Parameters 2-1: Cyanocysteine AMOEBA Parameters

```
atom         271   67    H1    "MeSCN H1"                    1     1.008    1
atom         272   68    C1    "MeSCN C1"                    6    12.011    4
atom         273   69    S     "MeSCN S"                    16    32.066    2
atom         274   70    C     "MeSCN C"                     6    12.011    2
atom         275   71    N     "MeSCN N"                     7    14.007    1

multipole    272  273  271              -0.22754
                                        0.00000   0.00000  -0.02449
                                        0.72145
                                        0.00000   0.72145
                                        0.00000   0.00000  -1.44290
multipole    273  272  274               0.33074
                                        0.44389   0.00000   0.28736
                                        1.22369
                                        0.00000  -2.16613
                                       -0.31636   0.00000   0.94244
multipole    274  273  275               0.24556
                                        0.06457   0.00000  -0.41800
                                        0.15740
                                        0.00000   0.22633
                                        0.26601   0.00000  -0.38373
multipole    271  272  273               0.07989
                                        0.02678   0.00000  -0.31473
                                        0.66454
                                        0.00000  -0.00998
                                        0.17231   0.00000  -0.65456
multipole    275  274  273              -0.58843
                                       -0.00512   0.00000  -0.24238
                                        0.32332
                                        0.00000   0.16836
                                       -0.08202   0.00000  -0.49168

polarize     271          0.4960     0.3900    272
polarize     272          1.3340     0.3900    271  273
polarize     273          3.3000     0.3900    272  274
polarize     274          1.3340     0.3900    273  275
polarize     275          1.0730     0.3900    274

vdw           68              3.7800     0.1060
vdw           69              4.0050     0.3550
vdw           70              3.7800     0.1060
vdw           67              2.8700     0.0330      0.900
vdw           71              3.7100     0.1050
bond          68   69        235.8000     1.8209
bond          68   67        341.0000     1.0794
bond          69   70        235.8000     1.7068
bond          70   71        450.0000     1.1373
angle         69   68   67    60.2400   110.5747
angle         67   68   67    39.5700   110.6263
angle         68   69   70    60.4300    99.4461
angle         69   70   71    60.0000   178.9042
strbnd        69   68   67    11.5000    11.5000
strbnd        68   69   70    -5.7500    -5.7500
torsion       67   68   69   70     0.0000 0.0 1  0.0000 180.0 2  0.6600 0.0 3
torsion       68   69   70   71     0.0000 0.0 1  0.0000 180.0 2  0.5000 0.0 3
```

Code and Parameters 2-2: Methyl Thiocyanate AMOEBA Parameters

```
atom         264   60    C1    "EtSCN C1"                    6    12.011    4
atom         265   61    H1    "EtSCN H1"                    1     1.008    1
atom         266   62    C2    "EtSCN C2"                    6    12.011    4
atom         267   63    H2    "EtSCN H2"                    1     1.008    1
atom         268   64    S     "EtSCN S"                    16    32.066    2
atom         269   65    C     "EtSCN C"                     6    12.011    2
atom         270   66    N     "EtSCN N"                     7    14.007    1

multipole    264  266  265             -0.18333
                                       0.00000   0.00000   0.32541
                                      -0.25019
                                       0.00000  -0.25019
                                       0.00000   0.00000   0.50038
multipole    266  264  268             -0.23503
                                       0.06819   0.00000   0.15097
                                      -0.26732
                                       0.00000  -0.08487
                                      -0.08743   0.00000   0.35219
multipole    267  266  264              0.09244
                                      -0.00077   0.00000  -0.03413
                                       0.02305
                                       0.00000   0.01348
                                      -0.00070   0.00000  -0.03653
multipole    265  264  266              0.08187
                                       0.01969   0.00000  -0.08459
                                       0.06966
                                       0.00000   0.02253
                                      -0.00032   0.00000  -0.09219
multipole    268  266  269              0.33074
                                       0.44389   0.00000   0.28736
                                       1.22369
                                       0.00000  -2.16613
                                      -0.31636   0.00000   0.94244
multipole    269  268  270              0.24556
                                       0.06457   0.00000  -0.41800
                                       0.15740
                                       0.00000   0.22633
                                       0.26601   0.00000  -0.38373
multipole    270  269  268             -0.58843
                                      -0.00512   0.00000  -0.24238
                                       0.32332
                                       0.00000   0.16836
                                      -0.08202   0.00000  -0.49168

polarize     264          1.3340     0.3900    265  266
polarize     265          0.4960     0.3900    264
polarize     266          1.3340     0.3900    264  267
polarize     267          0.4960     0.3900    266
polarize     268          3.3000     0.3900    269
polarize     269          1.3340     0.3900    268  270
polarize     270          1.0730     0.3900    269

vdw           60               3.8200     0.1040
vdw           62               3.7800     0.1060
```

```
vdw          64                4.0050     0.3550
vdw          65                3.7800     0.1060
vdw          63                2.8700     0.0330      0.900
vdw          61                2.9800     0.0240      0.920
vdw          66                3.7100     0.1050
bond         60   62         345.3000     1.5227
bond         60   61         341.0000     1.0855
bond         62   64         323.0000     1.8329
bond         62   63         341.0000     1.0809
bond         64   65         235.8000     1.7068
bond         65   66         450.0000     1.1376
angle        62   60   61     42.4400   111.1890
angle        61   60   61     39.5700   108.4478
angle        60   62   64     53.2000   114.3035
angle        60   62   63     42.4400   111.8003
angle        64   62   63     60.2400   108.0491
angle        63   62   63     45.5700   107.8321
angle        62   64   65     60.4300    99.8280
angle        64   65   66     60.0000   179.1383
strbnd       62   60   61     11.5000    11.5000
strbnd       60   62   64     18.7000    18.7000
strbnd       60   62   63     11.5000    11.5000
strbnd       64   62   63     11.5000    11.5000
strbnd       62   64   65     -5.7500    -5.7500
torsion      61   60   62   64     0.0000 0.0 1  0.0000 180.0 2  0.4750 0.0 3
torsion      61   60   62   63     0.0000 0.0 1  0.0000 180.0 2  0.2990 0.0 3
torsion      60   62   64   65    -0.4400 0.0 1 -0.2600 180.0 2  0.6000 0.0 3
torsion      63   62   64   65     0.0000 0.0 1  0.0000 180.0 2  0.6600 0.0 3
torsion      62   64   65   66     0.0000 0.0 1  0.0000 180.0 2  0.5000 0.0 3
```

Code and Parameters 2-3: Ethyl Thiocyanate AMOEBA Parameters

```
atom         276   72    C1    "HxSCN C1"                    6    12.011    4
atom         277   73    C2    "HxSCN C2"                    6    12.011    4
atom         278   74    H1    "HxSCN H1"                    1     1.008    1
atom         279   75    C3    "HxSCN C3"                    6    12.011    4
atom         280   76    H2    "HxSCN H2"                    1     1.008    1
atom         281   77    H3    "HxSCN H3"                    1     1.008    1
atom         282   78    C4    "HxSCN C4"                    6    12.011    4
atom         283   79    C5    "HxSCN C5"                    6    12.011    4
atom         284   80    H4    "HxSCN H4"                    1     1.008    1
atom         285   81    H5    "HxSCN H5"                    1     1.008    1
atom         286   82    C6    "HxSCN C6"                    6    12.011    4
atom         287   83    H6    "HxSCN H6"                    1     1.008    1
atom         288   84    S     "HxSCN S"                    16    32.066    2
atom         289   85    C     "HxSCN C"                     6    12.011    2
atom         290   86    N     "HxSCN N"                     7    14.007    1

multipole   279  282  277             -0.12665
                                      0.16365   0.00000   0.14302
                                      0.06092
                                      0.00000  -0.43628
                                     -0.27661   0.00000   0.37536
multipole   276  277  278             -0.15938
                                      0.00000   0.00000   0.26734
                                     -0.20136
                                      0.00000  -0.20136
                                      0.00000   0.00000   0.40272
multipole   283  282  286             -0.11656
                                      0.24230   0.00000   0.09285
                                      0.15205
                                      0.00000  -0.43470
                                     -0.43635   0.00000   0.28265
multipole   282  279  283             -0.11327
                                      0.22022   0.00000   0.08479
                                      0.15602
                                      0.00000  -0.44910
                                     -0.36114   0.00000   0.29308
multipole   277  279  276             -0.12195
                                      0.19367   0.00000   0.15795
                                     -0.01138
                                      0.00000  -0.31282
                                     -0.22362   0.00000   0.32420
multipole   286  283  288             -0.18161
                                      0.04843   0.00000   0.18545
                                     -0.01034
                                      0.00000  -0.10804
                                     -0.18618   0.00000   0.11838
multipole   280  277  279              0.05998
                                      0.00441   0.00000  -0.07636
                                      0.04595
                                      0.00000   0.03338
                                     -0.00973   0.00000  -0.07933
```

```
multipole   284  282  279               0.06214
                                       0.02649   0.00000  -0.05387
                                       0.01977
                                       0.00000   0.03305
                                      -0.00324   0.00000  -0.05282
multipole   281  279  282               0.05805
                                       0.00916   0.00000  -0.05550
                                       0.03877
                                       0.00000   0.02937
                                      -0.06123   0.00000  -0.06814
multipole   285  283  282               0.07555
                                       0.01936   0.00000  -0.04776
                                       0.05942
                                       0.00000   0.03376
                                      -0.01589   0.00000  -0.09318
multipole   278  276  277               0.05847
                                       0.01125   0.00000  -0.10159
                                       0.06569
                                       0.00000   0.03435
                                      -0.03952   0.00000  -0.10004
multipole   287  286  283               0.07235
                                       0.02117   0.00000  -0.04358
                                       0.04575
                                       0.00000   0.03869
                                      -0.01006   0.00000  -0.08444
multipole   288  286  289               0.33074
                                       0.44389   0.00000   0.28736
                                       1.22369
                                       0.00000  -2.16613
                                      -0.31636   0.00000   0.94244
multipole   289  288  290               0.24556
                                       0.06457   0.00000  -0.41800
                                       0.15740
                                       0.00000   0.22633
                                       0.26601   0.00000  -0.38373
multipole   290  289  288              -0.58843
                                      -0.00512   0.00000  -0.24238
                                       0.32332
                                       0.00000   0.16836
                                      -0.08202   0.00000  -0.49168

polarize    276          1.3340     0.3900    277  278
polarize    277          1.3340     0.3900    276  280
polarize    278          0.4960     0.3900    276
polarize    279          1.3340     0.3900    281
polarize    280          0.4960     0.3900    277
polarize    281          0.4960     0.3900    279
polarize    282          1.3340     0.3900    284
      polarize    283          1.3340     0.3900    285
      polarize    284          0.4960     0.3900    282
      polarize    285          0.4960     0.3900    283
      polarize    286          1.3340     0.3900    287
      polarize    287          0.4960     0.3900    286
      polarize    288          3.3000     0.3900    289
      polarize    289          1.3340     0.3900    288  290
      polarize    290          1.0730     0.3900    289

```

```
vdw          75                3.8200     0.1010
vdw          72                3.8200     0.1010
vdw          79                3.8200     0.1010
vdw          78                3.8200     0.1010
vdw          73                3.8200     0.1010
vdw          82                3.7800     0.1060
vdw          84                4.0050     0.3550
vdw          85                3.7800     0.1060
vdw          76                2.9800     0.0240      0.940
vdw          80                2.9800     0.0240      0.940
vdw          77                2.9800     0.0240      0.940
vdw          81                2.9800     0.0240      0.940
vdw          74                2.9600     0.0240      0.920
vdw          83                2.8700     0.0330      0.900
vdw          86                3.7100     0.1050
bond         75   78         453.0000     1.5299
bond         75   73         453.0000     1.5298
bond         75   77         341.0000     1.0885
bond         72   73         323.0000     1.5282
bond         72   74         341.0000     1.0863
bond         79   78         453.0000     1.5312
bond         79   82         345.3000     1.5276
bond         79   81         341.0000     1.0866
bond         78   80         341.0000     1.0879
bond         73   76         341.0000     1.0878
bond         82   84         235.8000     1.8351
bond         82   83         341.0000     1.0810
bond         84   85         235.8000     1.7063
bond         85   86         450.0000     1.1375
angle        78   75   73     48.2000   113.1072
angle        78   75   77     38.0000   109.3223
angle        73   75   77     38.0000   109.2787
angle        77   75   77     39.5700   106.3036
angle        73   72   74     42.4400   111.1869
angle        74   72   74     39.5700   107.7267
angle        78   79   82     48.2000   111.5264
angle        78   79   81     38.0000   109.6162
angle        82   79   81     38.0000   109.5120
angle        81   79   81     39.5700   106.9493
angle        75   78   79     48.2000   112.7564
angle        75   78   80     38.0000   109.3923
angle        79   78   80     38.0000   109.3217
angle        80   78   80     39.5700   106.4572
angle        75   73   72     48.2000   112.9179
angle        75   73   76     38.0000   109.3170
angle        72   73   76     38.0000   109.3845
angle        76   73   76     45.5700   106.3035
angle        79   82   84     53.2000   109.0812
angle        79   82   83     42.4400   111.1744
angle        84   82   83     60.2400   108.2095
angle        83   82   83     39.5700   108.8985
angle        82   84   85     60.4300    99.5693
angle        84   85   86     60.0000   179.0730
strbnd       78   75   73     18.7000    18.7000
strbnd       78   75   77     11.5000    18.7000
strbnd       73   75   77     11.5000    18.7000
strbnd       73   72   74     11.5000    11.5000
```

```
166.        strbnd        78   79   82    18.7000    18.7000
167.        strbnd        78   79   81    11.5000    18.7000
168.        strbnd        82   79   81    11.5000    18.7000
169.        strbnd        75   78   79    18.7000    18.7000
170.        strbnd        75   78   80    11.5000    18.7000
171.        strbnd        79   78   80    11.5000    18.7000
172.        strbnd        75   73   72    18.7000    18.7000
173.        strbnd        75   73   76    11.5000    18.7000
174.        strbnd        72   73   76    11.5000    18.7000
175.        strbnd        79   82   84    18.7000    18.7000
176.        strbnd        79   82   83    11.5000    11.5000
177.        strbnd        84   82   83    11.5000    11.5000
178.        strbnd        82   84   85    -5.7500    -5.7500
179.        torsion       73   75   78   79      0.576 0.0 1  -
    0.017 180.0 2   2.031 0.0 3
180.        torsion       73   75   78   80      0.000 0.0 1   0.000 180.0 2   0.000
    0.0 3
181.        torsion       77   75   78   79      0.000 0.0 1   0.000 180.0 2   0.000
    0.0 3
182.        torsion       77   75   78   80      0.000 0.0 1   0.000 180.0 2   0.000
    0.0 3
183.        torsion       78   75   73   72      0.484 0.0 1   0.014 180.0 2   2.221
    0.0 3
184.        torsion       78   75   73   76      0.000 0.0 1   0.000 180.0 2   0.000
    0.0 3
185.        torsion       77   75   73   72      0.000 0.0 1   0.000 180.0 2   0.000
    0.0 3
186.        torsion       77   75   73   76      0.000 0.0 1   0.000 180.0 2   0.000
    0.0 3
187.        torsion       74   72   73   75     0.0000 0.0 1  0.0000 180.0 2  0.3410
    0.0 3
188.        torsion       74   72   73   76     0.0000 0.0 1  0.0000 180.0 2  0.2990
    0.0 3
189.        torsion       82   79   78   75      0.364 0.0 1  -
    0.024 180.0 2   1.958 0.0 3
190.        torsion       82   79   78   80      0.000 0.0 1   0.000 180.0 2   0.000
    0.0 3
191.        torsion       81   79   78   75      0.000 0.0 1   0.000 180.0 2   0.000
    0.0 3
192.        torsion       81   79   78   80      0.000 0.0 1   0.000 180.0 2   0.000
    0.0 3
193.        torsion       78   79   82   84     -
    0.688 0.0 1   0.489 180.0 2   1.957 0.0 3
194.        torsion       78   79   82   83      0.000 0.0 1   0.000 180.0 2   0.000
    0.0 3
195.        torsion       81   79   82   84      0.000 0.0 1   0.000 180.0 2   0.000
    0.0 3
196.        torsion       81   79   82   83      0.000 0.0 1   0.000 180.0 2   0.000
    0.0 3
197.        torsion       79   82   84   85     -
    2.643 0.0 1   0.709 180.0 2   1.072 0.0 3
198.        torsion       83   82   84   85      0.000 0.0 1   0.000 180.0 2   0.000
    0.0 3
199.        torsion       82   84   85   86     0.0000 0.0 1  0.0000 180.0 2  0.5000
    0.0 3
```

Code and Parameters 2-4: Hexyl Thiocyanate AMOEBA Parameters

2.5 SMALL MOLECULE SIMULATIONS IN AMOEBA

<Body text to begin here.>

Chapter 3 Electrostatic Field Methods

3.1 AMBER03 WITH EXPLICIT TIP3P WATER

3.1.1 Reaction Field Electrostatics

3.1.2 Hybrid Solvent Reaction Field Electrostatics and Solute Coulomb Field

<Body text to begin here.>

3.2 AMBER03 WITH POISSON-BOLTZMANN CONTINUUM SOLVENT

3.2.1 Reaction Field Method

<Body text to begin here.>

3.2.2 Grid spacing and size

<Body text to begin here.>

3.2.3 Box Location

<Body text to begin here.>

3.3 AMBER03 WITH POISSON-BOLTZMANN CONTINUUM SOLVENT AND SELECT EXPLICIT TIP3P WATER MOLECULES

3.3.1 5 Å Water Sphere Around the Vibrational Chromophore

<Body text to begin here.>

3.3.2 Single Water Molecule Nearest the Vibrational Chromophore

<Body text to begin here.>

3.3.3 Water Molecular Hydrogen Bonding to the Vibrational Chromophore

<Body text to begin here.>

3.4 AMOEBA

3.4.1 Poisson-Boltzmann Continuum Solvent

<Body text to begin here.>

3.4.2 Explicit AMOEBA Water

<Body text to begin here.>

3.4.3 Charge Penetration Field Corrections

<Body text to begin here.>

Chapter 4 The Role of Electrostatics in Differential Binding of RalGDS to Rap Mutations E30D and K31E Investigated by Vibrational Spectroscopy of Thiocyanate Probes

4.1 Introduction

<Body text to begin here.>

4.2 Results

<Body text to begin here.>

4.3 Discussion

<Body text to begin here.>

Chapter 5 Optimizing Electrostatic Field Calculations with the Adaptive Poisson-Boltzmann Solver to Predict Electric Fields at Protein-Protein Interfaces I: Sampling and Focusing

5.1 Introduction

<Body text to begin here.>

5.2 Results

<Body text to begin here.>

5.3 Discussion

<Body text to begin here.>

Chapter 6 Optimizing Electrostatic Field Calculations with the Adaptive Poisson-Boltzmann Solver to Predict Electric Fields at Protein-Protein Interfaces II: Explicit Near-Probe and Hydrogen Bonding Water Molecules

6.1 Introduction

<Body text to begin here.>

6.2 Results

<Body text to begin here.>

6.3 Discussion

<Body text to begin here.>

Chapter 7 Electrostatic Fields at Protein-Protein Interfaces: Increased Sampling Time and Various Electrostatic Methods: A Case for Simulating in Polarizable Force Fields

7.1 Introduction

<Body text to begin here.>

7.2 Results

<Body text to begin here.>

7.3 Discussion

<Body text to begin here.>

Chapter 8 Electrostatic Fields in Small Thiocyanate Molecules with Ensembles Generated using the AMOEBA Force Field

8.1 Introduction

<Body text to begin here.>

8.2 Results

<Body text to begin here.>

8.3 Discussion

<Body text to begin here.>

Appendix

Glossary

This page is optional—must be placed in this order if it is included in the dissertation. If you don't want to include a glossary, then delete the entire page and the following page break.

References

1. Ensign, D. L.; Webb, L. J., Statistical, Geometric, and Physical Factors Determining Electrostatic Fields at the Ras/Effector Interface. **2010,** *in preparation*.
2. Stafford, A. J.; Ensign, D. L.; Webb, L. J., Vibrational Stark Effect Spectroscopy at the Interface of Ras and Rap1A Bound to the Ras Binding Domain of RalGDS Reveals an Electrostatic Mechanism for Protein-Protein Interaction. *J. Phys. Chem. B* **2010,** *114*, 15331-15344.
3. Van der Spoel, D.; Lindahl, E.; Hess, B.; Groenhof, G.; Mark, A. E.; Berendsen, H. J. C., Gromacs: Fast, Flexible, and Free. *J Comput Chem* **2005,** *26* (16), 1701-1718.
4. Geyer, M.; Herrmann, C.; Wohlgemuth, S.; Wittinghofer, A.; Kalbitzer, H. R., Structure of the Ras-binding domain of RalGEF and implications for Ras binding and signalling. *Nat. Struct. Biol.* **1997,** *4*, 694-699.
5. Huang, L.; Hofer, F.; Martin, G. S.; Kim, S. H., Structural basis for the interaction of Ras with RalGDS. *Nat. Struct. Biol.* **1998,** *5*, 422-426.
6. Nassar, N.; Horn, G.; Herrmann, C.; Scherer, A.; McCormick, F.; Wittinghofer, A., The 2.2 A crystal structure of the Ras-binding domain of the serine/threonine kinase c-Raf1 in complex with Rap1A and a GTP analogue. *Nature* **1995,** *375* (6532), 554-560.
7. Case, D. A.; Darden, T. A.; Cheatham, T. E.; Simmerling, C. L.; Wang, J.; Duke, R. E.; Luo, R.; Walker, R. C.; Zhang, W.; Merz, K. M., et al., *AMBER 11*. University of California, San Francisco: 2010.
8. Qamra, R.; Hubbard, S., - Structural basis for the interaction of the adaptor protein grb14 with activated. - *PLoS One. 2013 Aug 13;8(8):e72473. doi: 10.1371/journal.pone.0072473. eCollection* (- 1932-6203 (Electronic)).
9. Ensign, D. L.; Webb, L. J., Factors Determining Electrostatic Fields at the Ras/Effector Interface. *Proteins* **2011,** *79*, 3511-3524.
10. Ragain, C. M.; Newberry, R. W.; Ritchie, A. W.; Webb, L. J., Role of Electrostatics in Differential Binding of RaIGDS to Rap Mutations E30D and K31E Investigated by Vibrational Spectroscopy of Thiocyanate Probes. *J Phys Chem B* **2012,** *116* (31), 9326-9336.
11. Jorgensen, W. L.; Chandrasekhar, J.; Madura, J. D.; Impey, R. W.; Klein, M. L., Comparison of Simple Potential Functions for Simulating Liquid Water. *J Chem Phys* **1983,** *79* (2), 926-935.
12. Dolinsky, T. J.; Czodrowski, P.; Li, H.; Nielsen, J. E.; Jensen, J. H.; Klebe, G.; Baker, N. A., PDB2PQR: expanding and upgrading automated preparation of biomolecular structures for molecular simulations. *Nucleic Acids Res* **2007,** *35*, W522-W525.
13. Dolinsky, T. J.; Nielsen, J. E.; McCammon, J. A.; Baker, N. A., PDB2PQR: an automated pipeline for the setup of Poisson-Boltzmann electrostatics calculations. *Nucleic Acids Res* **2004,** *32*, W665-W667.

14. McCleverty, C. J.; Columbus, L.; Kreusch, A.; Lesley, S. A., Structure and ligand binding of the soluble domain of a Thermotoga maritima membrane protein of unknown function TM1634. *Protein Sci* **2008,** *17*, 869.
15. Humphrey, W.; Dalke, A.; Schulten, K., VMD - Visual Molecular Dynamics. *J. Molec. Graphics* **1996,** *14*, 33-38.
16. van der Spoel, D.; Lindahl, E.; Hess, B.; Groenhof, G.; Mark, A. E.; Berendsen, H. J. C., GROMACS: Fast, Flexible, and Free. *J. Comput. Chem.* **2005,** *26*, 1701-1718.
17. Smith, T. F.; Waterman, M. S., Identification of Common Molecular Subsequences. *J Mol Biol* **1981,** *147* (1), 195-197.
18. Russell, R. B.; Barton, G. J., Multiple protein sequence alignment from tertiary structure comparison. *PROTEINS: Struct. Funct. Genet.* **1992,** *14*, 309-323.
19. Duan, Y.; Wu, C.; Chowdhury, S.; Lee, M. C.; Xiong, G.; Zhang, W.; Yang, R.; Cieplak, P.; Luo, R.; Lee, T., et al., A Point-Charge Force Field for Molecular Mechanics Simulations of Proteins Based on Condensed-Phase Quantum Mechanical Calculations. *J. Comput. Chem.* **2003,** *24*, 1999-2012.
20. Darden, T.; York, D.; Pedersen, L. G., Particle mesh Ewald: An N log(N) method for Ewald sums in large systems. *J. Chem. Phys.* **1993,** *98*, 10089-10092.
21. Essmann, U.; Perera, L.; Berkowitz, M. L.; Darden, T.; Lee, H.; Pedersen, L. G., A smooth particle mesh Ewald method. *J. Chem. Phys.* **1995,** *103*, 8577-8593.
22. Hess, B.; Bekker, H.; Berendsen, H. J. C.; Fraaije, J. G. E. M., - LINCS: A linear constraint solver for molecular simulations. **1997,** - *18* (- 12), - 1472.
23. Roux, B., The calculation of the potential of mean force using computer simulations. *Comp. Phys. Commun.* **1995,** *91*, 275-282.
24. Gallicchio, E.; Andrec, M.; Felts, A. K.; Levy, R. M., Temperature Weighted Histogram Analysis Method, Replica Exchange, and Transition Paths. *J. Phys. Chem. B* **2005,** *109*, 6722-6731.